Supporting Information

Homochiral Dy_2 zero-field single-molecule magnets derived from axial chiral ligands (*R*)/(*S*)-octahydro-1,1′-bi-2-naphthyl phosphate

Cai-Ming Liu,*,† ,§ Xiang Hao,† and Yi-Quan Zhang*,§

†*Beijing National Laboratory for Molecular Sciences, CAS Key Laboratory for Organic Solids, Institute of Chemistry, Chinese Academy of Sciences, Beijing 100190, China. E-mail: cmliu@iccas.ac.cn*

§*Jiangsu Key Laboratory for NSLSCS, School of Physical Science and Technology, Nanjing Normal University, Nanjing 210023, China. E-mail: zhangyiquan@njnu.edu.cn*

Contents

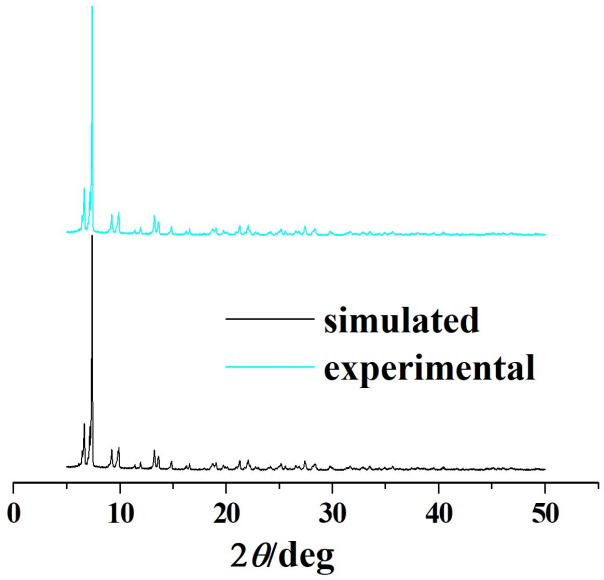

Fig. S1. The simulative and experimental powder X-ray diffraction patterns for *R*-**1.**

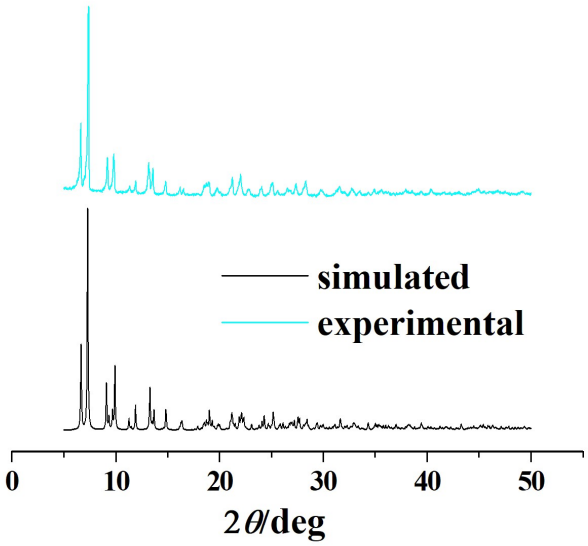

Fig. S2. The simulative and experimental powder X-ray diffraction patterns for *S*-**1.**

Table S1. Dy (III) ion geometry analysis by SHAPE 2.1 software for *S*-**1**.

Configuration	ABOXIY Dy1	ABOXIY Dy2
Octagon(D_{8h})	33.492	33.110
Heptagonal pyramid(C_{7v})	21.923	22.279
Cube (O_h)	12.026	12.106
Hexagonal bipyramid(D_{6h})	8.121	7.954
Square antiprism (D_{4d})	2.812	2.605
Triangular dodecahedron (D_{2d})	**1.923**	**1.881**
Johnson gyrobifastigium J26 (D_{2d})	12.565	12.637
Johnson elongated triangular bipyramid J14 (D_{3h})	27.237	26.490
Biaugmented trigonal prism J50 (C_{2v})	3.713	3.791
Biaugmented trigonal prism (C_{2v})	2.598	2.723
Snub diphenoid J84 (D_{2d})	5.389	5.336
Triakis tetrahedron (T_d)	8.900	8.774
Elongated trigonal bipyramid (D_{3h})	22.803	23.017

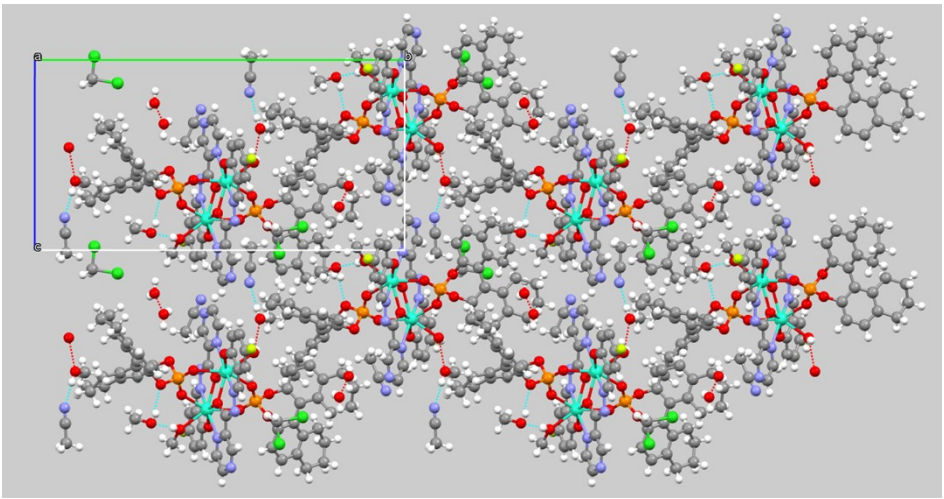

Fig. S3. The crystal packing diagram of *S*-**1**, viewed down the *a*-axis.

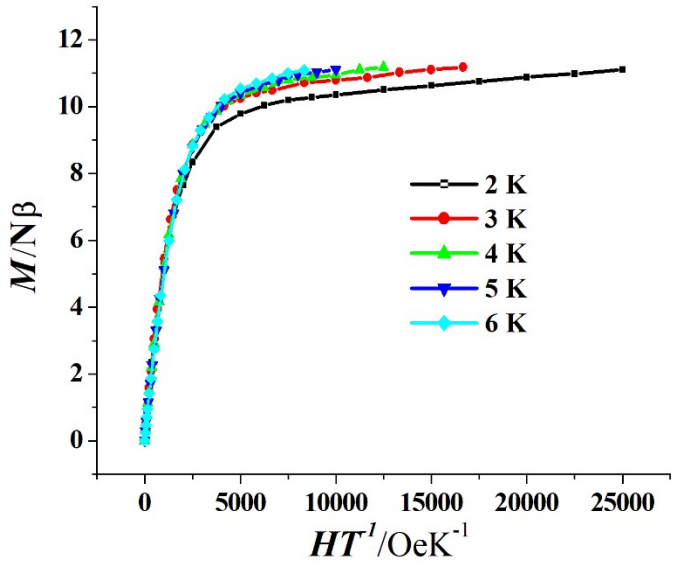

Fig. S4. *M versus H*/*T* plots at 2-6 K of *S*-**1**.

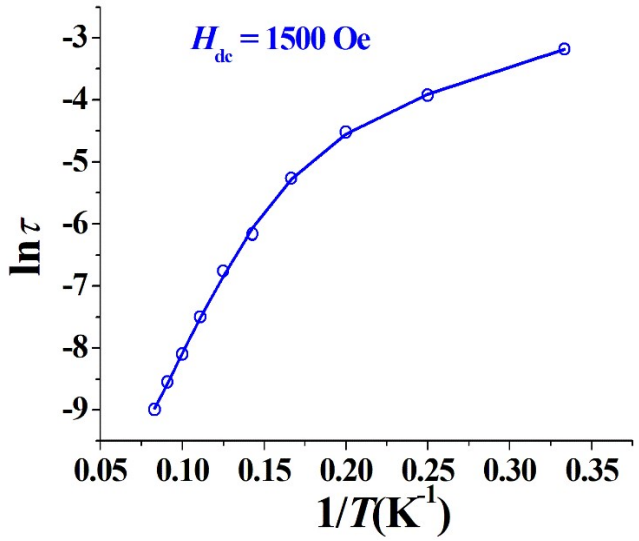

Fig. S5. Plot of lnτ *versus* 1/*T* for *S*-**1** (H_{dc} = 1500 Oe), the solid line represents the best fitting with Orbach *plus* Raman.

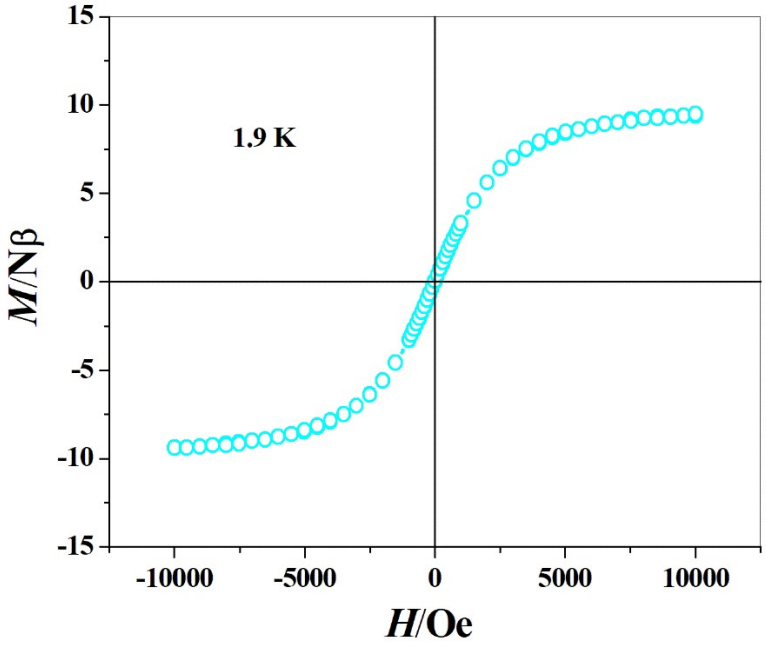

Fig. S6. Hysteresis loop for *S*-**1** at 1.9 K.

Computational details

For *S*-**1**, we need to calculate two individual Dy^{III} fragments due to their unsymmetrical structures. Complete-active-space self-consistent field (CASSCF) calculations on two individual Dy^{III} fragments for *S*-**1** (Fig. S5) on the basis of single-crystal X-ray determined geometry have been carried out with the OpenMolcas[S1] program package. Each individual Dy^{III} fragment in *S*-**1** was calculated keeping the experimentally determined structure of the corresponding compound while replacing the neighboring Dy^{III} ion by diamagnetic Lu^{III}.

The basis sets for all atoms are atomic natural orbitals from the OpenMolcas[S1] ANO-RCC library: ANO-RCC-VTZP for Dy^{III}; VTZ for close N and O; VDZ for distant atoms. The calculations employed the second order Douglas-Kroll-Hess Hamiltonian, where scalar relativistic contractions were taken into account in the basis set and the spin-orbit couplings were handled separately in the restricted active space state interaction (RASSI-SO) procedure.[S2–S3] Active electrons in 7 active orbitals include all *f* electrons (CAS (9 in 7) in the CASSCF calculation. To exclude all the doubts, we calculated all the roots in the active space. We have mixed the maximum number of spin-free state which was possible with our hardware (all from 21 sextets, 128 from 224 quadruplets, 130 from 490 doublets for Dy^{III}. SINGLE_ANISO[S4–S6] program was used to obtain the energy levels, ***g*** tensors, magnetic axes, *et al.* based on the above CASSCF/RASSI-SO calculations.

To fit the exchange interactions in *S*-**1**, we took two steps to obtain them. Firstly, we calculated individual Dy^{III} fragments using CASSCF/RASSI-SO to obtain the corresponding magnetic properties. Then, the exchange interaction between the magnetic centers was considered within the Lines model,[S7] while the account of the dipole-dipole magnetic coupling was treated exactly. The Lines model is effective and has been successfully used widely in the research field of *d* and *f*-elements single-molecule magnets.[S8-S9]

S-**1** has one type of $\mathcal{J}$. The Ising exchange Hamiltonian is:

$$\hat{H}_{exch} = -\tilde{J}\hat{\tilde{S}}_{Dy1}\hat{\tilde{S}}_{Dy1'} \qquad \text{(S1)}$$

$\mathcal{J} = 25\cos\varphi J$, where φ is the angle between the magnetic axes on two Dy^{III} sites, and J is the Lines exchange coupling parameter. $\tilde{S}_{Dy} = 1/2$ is the ground pseudospin on the Dy^{III} site. $\mathcal{J}_{total}$ is the parameter of the total magnetic interaction ($\mathcal{J}_{total} = \mathcal{J}_{dip} + \mathcal{J}_{exch}$) between magnetic center ions. The dipolar magnetic coupling can be calculated exactly, while the exchange coupling constant was fitted through comparison of the computed and measured magnetic susceptibilities using the POLY_ANISO program.[S4-S6]

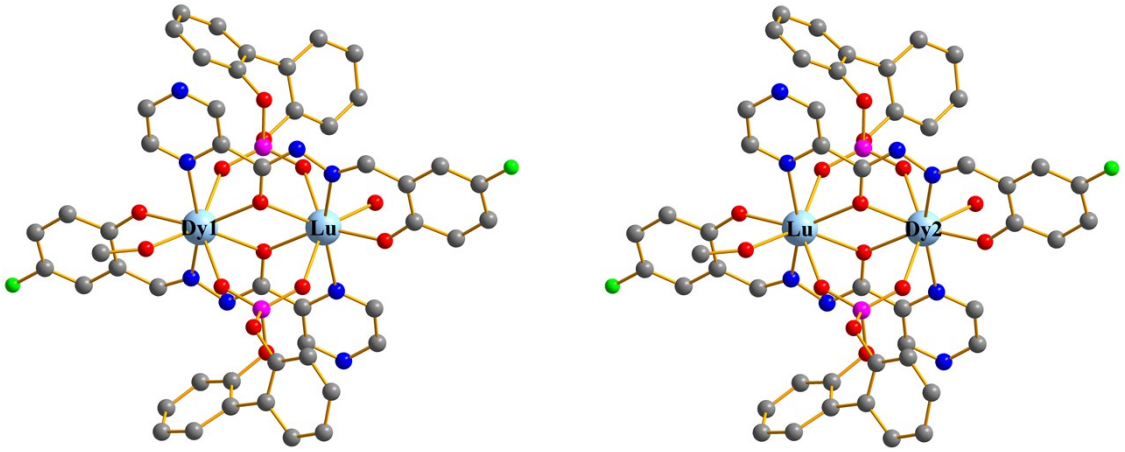

Dy1 Dy2

Fig. S7. Calculated complete structures of *S*-**1**; H atoms are omitted for clarify.

Table S2. Calculated energy levels (cm^{-1}), $\boldsymbol{g}$ (g_x, g_y, g_z) tensors and predominant m_J values of the lowest eight Kramers doublets (KDs) of individual Dy^{III} fragments for *S*-**1** using CASSCF/RASSI-SO with the OpenMolcas.

KDs	Dy1			Dy2		
	E/cm^{-1}	$\boldsymbol{g}$	m_J	E/cm^{-1}	$\boldsymbol{g}$	m_J
0	0.0	0.015 0.019 19.712	±15/2	0.0	0.009 0.011 19.738	±15/2
1	163.0	0.215 0.274 16.836	±13/2	179.3	0.159 0.190 16.897	±13/2
2	301.1	2.139 3.307 12.408		340.2	1.481 2.176 12.987	
3	376.7	9.516 5.292 0.521		428.9	0.736 3.809 10.754	
4	439.2	2.104 3.127 15.209		505.9	2.234 3.862 13.106	
5	486.4	0.042 2.324 13.386		539.0	0.302 2.703 13.832	
6	545.4	1.046 2.060 16.145		603.8	0.146 2.721 15.336	
7	602.5	0.169 0.612 17.935		646.1	0.620 2.171 17.185	

Table S3. Wave functions with definite projection of the total moment | m_J > for the lowest eight KDs of individual Dy^{III} fragments for *S*-**1**.

	E/cm^{-1}	wave functions
Dy1	0.0	98%|±15/2>
	163.0	93.6%|±13/2>
	301.1	74.5%|±11/2>+7.9%|±5/2>+5.8%|±3/2>+5.2%|±7/2>
	376.7	40.1%|±9/2>+18.7%|±1/2>+18.3%|±3/2>+9.1%|±11/2>+8.6%|±5/2>
	439.2	24.8%|±1/2>+23.3%|±7/2>+18.3%|±9/2>+14.6%|±3/2>+14%|±5/2>
	486.4	23.3%|±9/2>+21.6%|±5/2>+20.9%|±7/2>+19.9%|±3/2>+9.5%|±1/2>
	545.4	38.6%|±1/2>+24.1%|±7/2>+18.2%|±3/2>+13.7%|±5/2>
	602.5	32.7%|±5/2>+23%|±3/2>+20.1%|±7/2>+12.1%|±9/2>+6.3%|±11/2>
Dy2	0.0	98.3%|±15/2>
	179.3	94.3%|±13/2>
	340.2	78.9%|±11/2>+7.3%|±7/2>+4.6%|±3/2>
	428.9	42.6%|±9/2>+18.7%|±3/2>+16.7%|±1/2>+7.6%|±5/2>+7.3%|±11/2>
	505.9	28.7%|±1/2>+23.4%|±7/2>+19.4%|±9/2>+12.2%|±3/2>+11.7%|±5/2>
	539.0	22.5%|±5/2>+21.5%|±9/2>+20.4%|±3/2>+18.5%|±7/2>+14%|±1/2>
	603.8	31.5%|±1/2>+29.5%|±7/2>+19.2%|±3/2>+14.3%|±5/2>
	646.1	35.7%|±5/2>+24.8%|±3/2>+16.9%|±7/2>+10.2%|±9/2>+5.8%|±1/2>

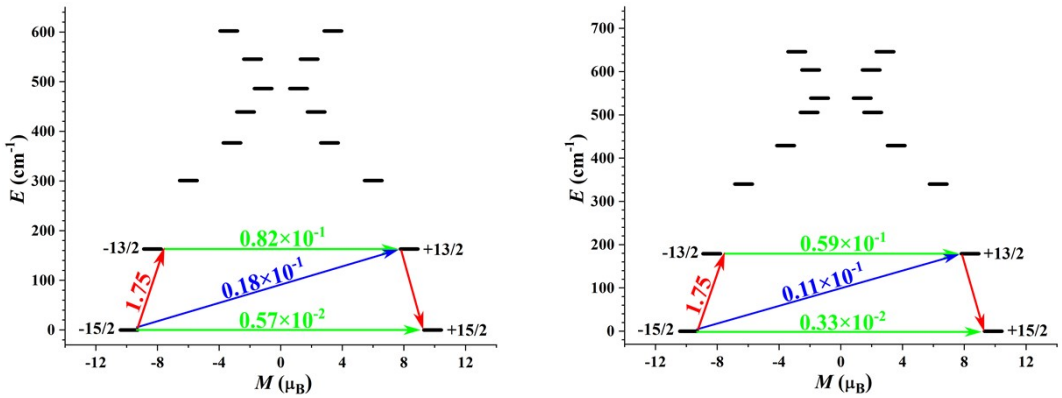

Dy1 Dy2

Fig. S8. Magnetization blocking barriers of individual Dy^{III} fragments for *S*-**1**. The thick black lines represent the KDs as a function of their magnetic moment along the magnetic axis. The green lines correspond to diagonal quantum tunneling of magnetization (QTM); the blue line represent off-diagonal relaxation process. The numbers at each arrow stand for the mean absolute value of the corresponding matrix element of transition magnetic moment.

Table S4. Exchange energies E (cm^{-1}), the energy difference between each exchange doublets Δ_t (cm^{-1}) and the main values of the g_z for the lowest two exchange doublets of *S*-**1**.

	E	Δ_t	g_z
1	0.000000000000	0.849×10^{-7}	39.439
	0.000000084949		
2	3.010867490053	0.804×10^{-7}	0.926
	3.010867570411		

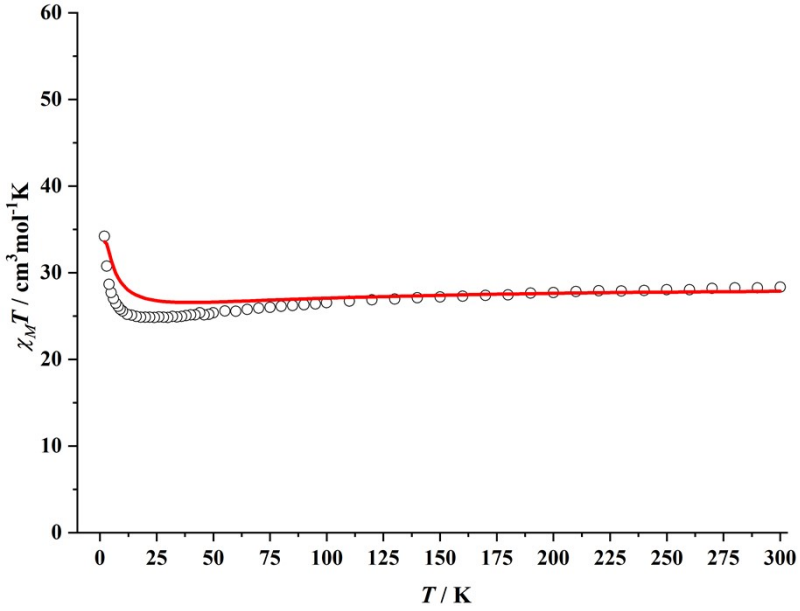

Fig. S9. Calculated (red solid line) and experimental (black square dot) data of magnetic susceptibilities of *S*-**1**. The intermolecular interactions zJ' of *S*-**1** were fitted to –0.02 cm^{-1}.

References:

S1 Galván, I. F.; Vacher, M.; Alavi, A.; Angeli, C.; Aquilante, F.; Autschbach, J.; Bao, J. J.; Bokarev, S. I.; Bogdanov, N. A.; Carlson, R. K.; Chibotaru, L. F.; Creutzberg, J.; Dattani, N.; Delcey, M. G.; Dong, S. S.; Dreuw, A.; Freitag, L.; Frutos, L. M.; Gagliardi, L.; Gendron, F.; Giussani, A.; González, L.; Grell, G.; Guo, M. Y.; Hoyer, C. E.; Johansson, M.; Keller, S.; Knecht, S.; Kovacevic, G.; Källman, E.; Manni, G. L.; Lundberg, M.; Ma, Y. J.; Mai, S.; Malhado, J. P.; Malmqvist, P. Å.; Marquetand, P.; Mewes, S. A.; Norell, J.; Olivucci, M.; Oppel, M.; Phung, Q. M.; Pierloot, K.; Plasser, F.; Reiher, M.; Sand, A. M.; Schapiro, I.; Sharma, P.; Stein, C. J.; Sørensen, L. K.; Truhlar, D. G.; Ugandi, M.; Ungur, L.; Valentini, A.; Vancoillie, S.;

Veryazov, V.; Weser, O.; Wesołowski, T. A.; Widmark, Per-Olof.; Wouters, S.; Zech, A.; Zobel, J. P.; Lindh. R. *J. Chem. Theory Comput.* **2019**, *15*, 5925–5964.

S2 Malmqvist, P. Å.; Roos, B. O.; Schimmelpfennig, B. *Chem. Phys. Lett.,* **2002**, *357,* 230–240.

S3 Heß, B. A.; Marian, C. M.; Wahlgren, U.; Gropen, O. *Chem. Phys. Lett.,* **1996**, *251,* 365–371.

S4 Chibotaru, L. F.; Ungur, L.; Soncini, A. *Angew. Chem., Int. Ed*. **2008**, *47*, 4126–4129.

S5 Ungur, L.; Van den Heuvel, W.; Chibotaru, L. F. *New J. Chem.* **2009**, *33*, 1224–1230.

S6 Chibotaru, L. F.; Ungur, L.; Aronica, C.; Elmoll, H.; Pilet, G.; Luneau, D. *J. Am. Chem. Soc*. **2008**, *130*, 12445–12455.

S7 Lines, M. E. *J. Chem. Phys*. **1971**, *55*, 2977−2984.

S8 Mondal, K. C.; Sundt, A.; Lan, Y. H.; Kostakis, G. E.; Waldmann, O.; Ungur, L.; Chibotaru, L. F.; Anson, C. E.; Powell, A. K. *Angew. Chem., Int. Ed.* **2012**, *51*, 7550−7554.

S9 Langley, S. K.; Wielechowski, D. P.; Vieru, V.; Chilton, N. F.; Moubaraki, B.; Abrahams, B. F.; Chibotaru, L. F.; Murray, K. S. *Angew. Chem., Int. Ed.* **2013**, *52*, 12014–12019.

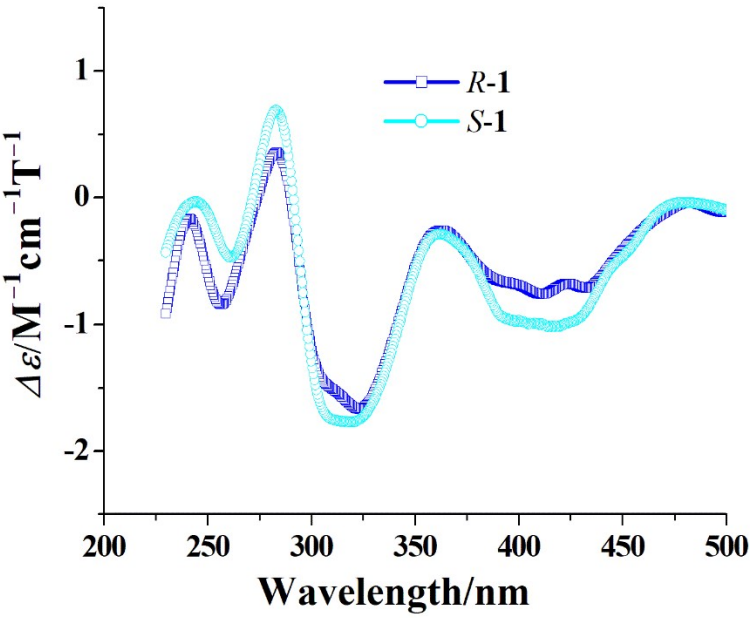

Fig. S10. MCD spectra of *R*-**1** and *S*-**1**.